Charge Distribution Produced by 4- to 24-MeV Electrons in Elemental Materials

Tatsuo Tabata, Rinsuke Ito, and Shigeru Okabe
Radiation Center of Osaka Prefecture, Sakai, Osaka, Japan

and

Yoshiaki Fujita
Research Reactor Institute, Kyoto University, Kumatori, Osaka, Japan

(Received 22 April 1970)

Charge-deposition distributions of monoenergetic electrons normally incident on thick absorbers of Be, Al, Cu, Ag, and Au have been measured with a thin collector moved through the absorber thickness. The measurements have been made at incident energies of 4.09, 7.79, 11.5, and 14.9 MeV, and also at 23.5 MeV for absorbers other than Be. Values of the most probable charge-deposition depth x_m and the charge-deposition straggling w have been determined from the distributions observed. The ratio of x_m to the theoretical mean range L of the incident electrons decreases with decreasing incident energy E_0 and with increasing atomic number Z of the absorber, reflecting the effect of multiple-scattering detours of the primary electrons. The ratio w/L shows an increase with increasing E_0 in the region of $E_0 \gtrsim 11$ MeV for Al and in the entire energy region of the present experiment for Cu, Ag, and Au; this trend is considered mainly due to bremsstrahlung energy-loss straggling. The contribution to the measured distributions of electrons mediated by bremsstrahlung has been found to be less than about 1×10^{-3} cm^2/g absorbed electron. Some of the distributions are compared with the Monte Carlo results of Berger and Seltzer. Agreement between the experimental and calculated results is rather good except in the case of the Be absorber.

I. INTRODUCTION

Energetic electrons incident to a target suffer energy loss and scattering, and some of them are eventually absorbed by the target. Some secondary electrons, either liberated by the incident electrons or mediated by bremsstrahlung, also come to a stop in the target. As a consequence of the statistical nature of the energy-loss and scattering processes, the electric charge thus deposited shows a distribution along the depth of the target. This distribution is called charge-deposition distribution produced by (or, for simplicity, charge distribution of) the incident electrons in the target, and is of growing interest in relation to charge buildup in material, particularly in insulators. From another point of view, the charge-deposition distribution is one of the problems of deep penetration of electrons, complete theoretical treatment of which is very difficult because of the mathematical complexities involved.

Early works on the penetration of fast electrons through matter have been reviewed by Birkhoff.[1] Since the appearance of this review, the effectiveness of the Monte Carlo method in solving transport problems of electrons has been demonstrated by a number of authors.[2-10] Among them, Berger and Seltzer have developed a Monte Carlo code which permits one to compute the charge distribution of electrons in various materials.[8,10] Kessaris[11] has calculated the charge distribution of electrons in water by the use of the moment method; the first successful application of this method to electron transport was made by Spencer.[12]

Experimentally, Gross and Wright[13] obtained the charge distribution of 3-MeV electrons in Plexiglass and Al using a thin charge collector inserted in the absorber. Similar measurements were made for 4- to 25-MeV electrons in water, oil, and Al by Alexander *et al.*,[14] and for 20-MeV electrons in polystyrene by Laughlin.[15] An extension of the measurement for other elemental materials covering a wide region of atomic number is desirable to provide a suitable spread of check points for theoretical treatments.

The present work describes an experiment in which a systematic measurement of the charge distribution of electrons was made in the region of incident energy from 4.09 to 23.5 MeV for the absorbers of Be, Al, Cu, Ag, and Au. Preliminary accounts of this work have been given previously.[16,17] The results are compared with the recent Monte Carlo calculations of Berger and Seltzer.[18]

II. EXPERIMENTAL

A. General

Consider an electron beam normally incident to the plane surface of an absorber extending in a semiinfinite half-space $x \geq 0$. Let us assume that the region from $x - \Delta x/2$ to $x + \Delta x/2$ is electrically insulated from the rest of the absorber so as to serve as a charge collector. Under this geometry we can measure the charges $\Delta q(x)$ and $Q(x)$ due to

net absorption of the electrons in the collector and the rest of the absorber, respectively; the net charge absorbed by the whole absorber is given by their sum. Then, the ratio $y(x)\,dx$ of the net charge, deposited in a layer of thickness dx at the depth x, to the total charge of the *electrons absorbed* by the whole absorber is determined from

$$y(x)\,dx = \Delta q(x)\,dx/[\Delta q(x) + Q(x)]\Delta x\,. \quad (1)$$

The ratio $y_0(x)\,dx$ of the same net charge in dx to the total charge of the *incident electrons* is given by

$$y_0(x)\,dx = (1-\eta)y(x)\,dx\,, \quad (2)$$

where η is the backscattering coefficient at saturation of the incident electrons for the absorber material considered. Since $y(x)$ and $y_0(x)$ are the same aside from a constant multiplication factor, the present results will be given in $y(x)$. Values of $y_0(x)$ will be used only when the experimental data are compared with the Monte Carlo results.

B. Electron Beam

The electron beam used in this experiment was produced by the linear accelerator of the Radiation Center of Osaka Prefecture (RCO) for energies up to 14.9 MeV and by the linear accelerator of the Kyoto University Research Reactor Institute (KURRI) for 23.5 MeV. In the experiment at RCO, about 0.03–1 μA of the beam, analyzed in energy to 1% with a magnet, was brought into the experimental area through a shielding wall. A pair of quadrupole magnets focused the beam on a tantulum-edged copper collimator 5.5 m away. The aperture of the collimator was 0.6 cm diam, and the angular divergence of the beam was less than 0.05°. The beam admitted by the collimator passed through a 0.027-g/cm^2 aluminum window at a distance of 70 cm from the collimator, and then impinged on the absorber system at 1.9 cm from the window. The experiment at KURRI was performed with a similar arrangement. Differences to be noted were the following: No shielding wall was provided between the analyzing magnet and the experimental area; the thickness of the aluminum window was 0.054 g/cm^2; and the distance between the window and the absorber system was 7.6 cm.

C. Energy Calibration

The energy scale of the analyzing magnet of RCO was calibrated within an error of 0.4% by measuring the conversion line of Cs^{137} and the threshold of the Cu^{63} (γ,n) reaction. Calibration of the KURRI analyzing magnet was made as follows: The charge distribution of electrons in Al was measured for the electrons of about 14 MeV from the KURRI accelerator. Various experimental projected ranges were determined from this distribution. By comparing these results with the range-energy relations obtained from the RCO experiment,[16,17] the energy scale was determined within an error of 0.6%.

D. Absorber System

The experimental arrangement near the absorber system is shown schematically in Fig. 1. The absorbers used were in the form of a disk 3–13 cm in diameter, and were better than 99.7% pure. The total thickness and the diameter of the absorbers in each case were made large enough for the absorber assembly to be regarded as effectively semi-infinite. The collector, consisting of disks of the same material as the absorber, was put in an insulating sheath made of 0.0035-g/cm^2 Mylar film, which in turn was placed between the absorbers. The thickness of the collector used varied from about 0.07 to 0.5 g/cm^2, approximately in proportion to incident energy. A 0.008-cm-diam enamel-coated copper wire, one end of which was inserted in the insulating sheath, served for electrical connection between the collector and the coaxial cable leading to the measuring area. In order to reduce the charge loss due to escape of the secondary electrons produced by bremsstrahlung, lead disks either 6 or 13 cm in diameter and 5 cm in total thickness were placed behind the absorber assembly. The entire system was insulated with Plexiglass plates (not shown in Fig. 1) and was attached to the window flange.

E. Charge Measurement

Currents from the collector and the absorber assembly were respectively amplified with picoammeters, and then were fed to current integrators. The feedback network of the picoammeters kept the input voltage drop less than 1 mV, so that the collection of air ionization current due to the appearance of a voltage on the absorber assembly

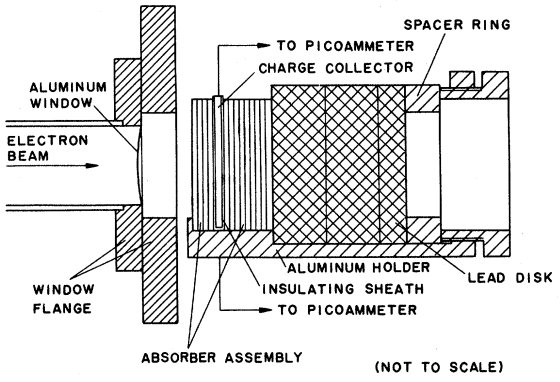

FIG. 1. Schematic diagram showing the experimental arrangement near the absorber system.

or the collector was minimized. Current integration was started with a master switch simultaneously in the two integrators. When the charge from the absorber assembly reached a value predetermined for the first integrator, it generated a signal-to-stop integration in the second integrator and to trigger a digital voltmeter, which provided precision reading of the charge accumulated in the latter integrator.

F. Background

Bremsstrahlung x rays, which came from the collimator and the analyzer slits in the RCO and the KURRI experiments, respectively, liberated electrons in passing through the absorber system and surroundings. These electrons caused collection of background charges from (i) the signal line connected to the collector and the absorber assembly, and (ii) the body of the absorber system. The background from the collector line was measured by removing the collector from the insulating sheath, and was found to be 0.01–0.6% of the maximum of the collector charge $\Delta q(x)$ in each charge distribution. This background was subtracted to obtain the net collector charge. The background charge from the absorber-assembly line was of the same order of magnitude as the background from the collector line, and it could be neglected compared with true signals from the absorber assembly.

The background from the body of the absorber system was not measured directly, but was checked by evaluating the integral of the charge distribution $y_{obs}(x)$ observed,

$$Y = \int_0^{x_{max}} y_{obs}(x)\,dx, \tag{3}$$

where x_{max} is a thickness beyond which the contribution of the integrand is considered to be negligible. The definition of $y(x)$ as given by Eq. (1) requires that Y be equal to unity. If the background of the second type is appreciable, however, this requirement will not be satisfied, because the background charge deposited in the region of the absorber system not scanned by the collector [i.e., in the deepest part of the absorber assembly ($x > x_{max}$), in the lead shielding, and in the aluminum holder] will produce a difference of Y from unity. Thus, this difference gives a measure of the background of the second type. In the case of the RCO experiment, Y was found to be unity within an error of 0.8%. Therefore, the background of this type could be considered almost negligible. For the KURRI experiment, an apparent deviation of the same sign was observed (−6.1% average), indicating the presence of appreciable background. The higher level of the background in the KURRI experiment was due to the higher energy used and the absence of the shielding wall to isolate the experimental area. Errors introduced by this background can be separated into two types: possible distortion of the distribution and rather trivial errors in the scale factor. The former was taken into account in the probable errors in $y(x)$ (see Sec. IV); the latter were corrected by the normalization procedure (see Sec. III).

III. TREATMENT OF DATA AND DEFINITION OF PARAMETERS

In scaling the depth x, the distribution $y(x)$, and quantities derived from it, the mean range L of the incident electrons will frequently be used; it is defined as the range computed in the continuous slowing-down approximation according to the equation

$$L = \int_0^{E_0} \rho \left(-\frac{dE}{ds}\right)^{-1} dE, \tag{4}$$

where ρ is the density of the absorber material and $-dE/ds$ is the mean energy loss of electrons per unit path length.

Total thickness of the aluminum window, intervening air, and Mylar film in front of the collector was included in the values of x. This correction amounted to 0.033 and 0.067 g/cm^2 for the RCO and the KURRI arrangements, respectively, and was 0.4–1.3% of L.

A systematic error is possibly introduced into the scale factor of $y(x)$ by the following causes: background of the second type described in Sec. II F, uncertainty in the relative calibration of the current-integration systems, and uncertainty in the determination of collector thickness. In order to minimize this error, the observed values $y_{obs}(x)$ were divided by Y, which was obtained for each distribution through numerical evaluation of the right-hand side of Eq. (3).

From the curve of $y(x)$ thus obtained, the following parameters characterizing the distribution were determined: (i) The most probable charge-deposition depth x_m: the depth at which $y(x)$ attains its maximum; (ii) the charge-deposition straggling w: full width at half-maximum (FWHM) of $y(x)$. Values of w were obtained from the observed FWHM w_{obs} of the distribution by applying a correction for finite thickness Δx of the charge collector:

$$w^2 = w_{obs}{}^2 - \Delta x^2. \tag{5}$$

This correction, however, was less than 0.5%.

Values of η required for converting $y(x)$ to $y_0(x)$ were determined through interpolation or extrapolation from Tabata's experimental results,[19] which are in good agreement with later results of Harder and Metzger[20] and of Ebert *et al.*[21] The values used are presented in Table I.

TABLE I. Values of backscattering coefficient η used in converting $y(x)$ to $y_0(x)$. E_0 is the incident-electron energy.

Absorber	E_0 (MeV)	η (%)
Be($Z=4$)	11.5	0.1
Al($Z=13$)	4.09	3.2
	7.79	1.3
	11.5	0.9
Cu($Z=29$)	11.5	3.1
Ag($Z=47$)	11.5	6.2
Au($Z=79$)	11.5	10.9

IV. ACCURACY

The probable errors in the values of $y(x)$ determined in this experiment are given in Table II as the sum of two terms; one is a constant in a distribution, and the other is proportional to $y(x)$. The first consists of the uncertainty in the correction of the background from the signal line connected to the collector (this and the other corrections described below were assumed to be uncertain by ±30%), and for 23.5 MeV it also includes the uncertainty due to the background from the body of the absorber system. Estimation of the latter uncertainty was made by using the difference of the integral Y from unity on the assumption that the spatial distribution of the bremsstrahlung x rays from the analyzer slits was approximately uniform around the absorber system, producing a nearly constant deposition of background charge along the depth; this assumption may be justified because of high penetrability of the x rays and the large distance of about 3 m between the analyzer slits and the absorber system. The second term of the errors includes the effect of fluctuation, the main cause of which is considered to be related to charge buildup and occasional discharge in the insulating sheath. The uncertainty due to this fluctuation was estimated to be about 3.8% from the standard deviation about the mean of the values measured for the same point and from the scattering of neighboring points around a smooth curve. Another error included in the second term is that due to the uncertainty in the correction of the scale factor, and is significant only for 23.5 MeV (1.0–3.3%). Possible error due to the finite thickness Δx of the collector is not included in the probable errors listed in Table II. It is considered appreciable only for the point of smallest depth in each distribution, around which the instrumental resolution as determined by Δx was not enough because of rapid change of $y(x)$.

An additional error is introduced into the values of $y_0(x)$ by the uncertainty of about ±10% in η. In the cases shown in Figs. 2–6, however, the errors in $y_0(x)$ are almost the same as those in the corresponding values of $y(x)$ on account of rather small values of η.

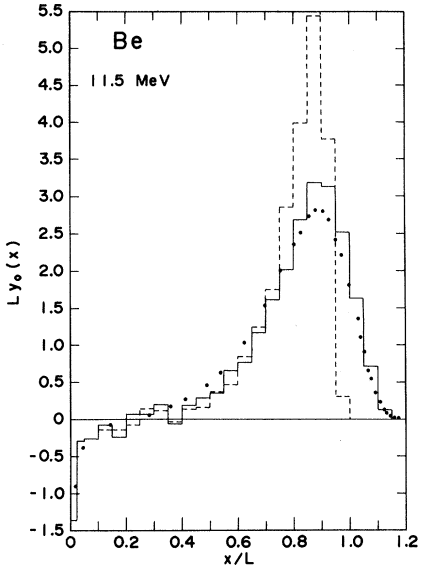

FIG. 2. Measured charge distribution of 11.5-MeV electrons in Be is shown by solid circles. Histograms represent the Monte Carlo results of Berger and Seltzer for 10 MeV. Energy loss of electrons was treated in the continuous slowing-down approximation for the dashed histogram, and energy-loss straggling was included in the calculation for the solid histogram.

TABLE II. Probable errors in $y(x)$ expressed in units of 10^{-1} cm^2/g absorbed electron. y stands for the value of $y(x)$ in the same units.

E_0	Error				
(MeV)	Be($Z=4$)	Al($Z=13$)	Cu($Z=29$)	Ag($Z=47$)	Au($Z=79$)
4.09	±(0.002+0.038y)	±(0.001+0.038y)	±(0.001+0.038y)	±(0.002+0.038y)	±(0.001+0.038y)
7.79	±(0.001+0.039y)	±(0.001+0.038y)	±(0.001+0.038y)	±(0.002+0.038y)	±(0.001+0.038y)
11.5	±(0.001+0.038y)	±(0.001+0.038y)	±(0.001+0.039y)	±(0.001+0.038y)	±(0.004+0.038y)
14.9	±(0.001+0.038y)	±(0.001+0.038y)	±(0.001+0.038y)	±(0.001+0.038y)	±(0.001+0.038y)
23.5	...	±(0.020+0.050y)	±(0.003+0.040y)	±(0.002+0.039y)	±(0.002+0.043y)

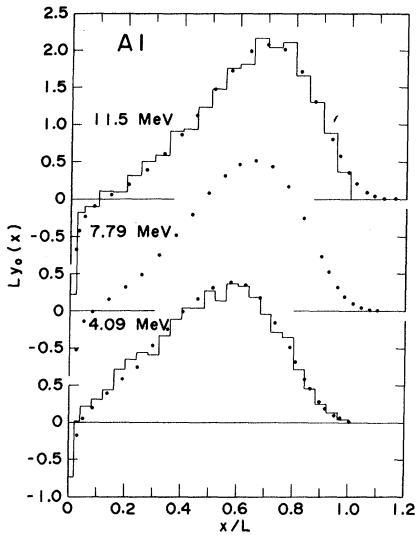

FIG. 3. Measured charge distributions of 4.09-, 7.79-, and 11.5-MeV electrons in Al are shown by solid circles. Histrograms represent the Monte Carlo results of Berger and Seltzer for 4 and 10 MeV. The absorber configuration assumed for the latter energy is the finite slab of thickness equal to L.

The errors in the parameters x_m and w consist of the uncertainties in the energy calibration described in Sec. IIC, in the measurement of absorber thickness (0.1–0.3%), and in the interpolation of the distribution curve through the experimental points (0.4–5.5%). The errors in x_m further include the uncertainty in the correction for the thickness of intervening layers of the aluminum window, etc., described in Sec. III. Limits on the accuracy of the parameters expressed in per cent as a probable error are x_m: 0.6–3.0%; and w: 1.6–5.6%.

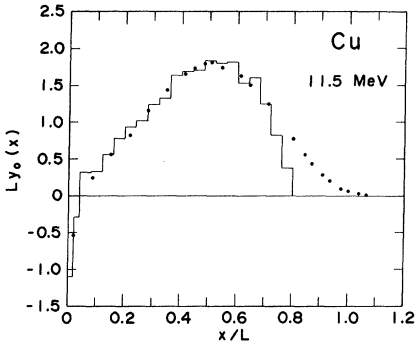

FIG. 4. Measured charge distribution of 11.5-MeV electrons in Cu is shown by solid circles. Histogram represents the Monte Carlo result of Berger and Seltzer for 10 MeV and the finite slab of thickness 0.8L.

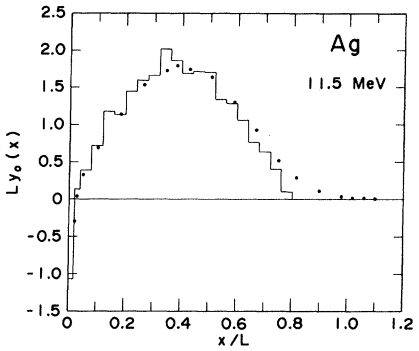

FIG. 5. Measured charge distribution of 11.5-MeV electrons in Ag is shown by solid circles. Histogram represents the Monte Carlo result of Berger and Seltzer for 10 MeV and the finite slab of thickness 0.8L.

V. RESULTS AND DISCUSSION

The charge distribution was measured for Be, Al, Cu, Ag, and Au at incident energies of 4.09, 7.79, 11.5, 14.9, and 23.5 MeV. The measurement for Be was excluded at 23.5 MeV, because the diameter and the total thickness of the absorbers used were insufficient at this energy. The results are shown in Tables III-VII, and graphical representation of typical distributions is given in Figs. 2–6. The ordinate and the abscissa of these figures are in dimensionless parameters of $Ly_0(x)$ and x/L, respectively. Values used of the mean range L were obtained through interpolation from the table of Berger and Seltzer,[22] and are given in column 3 of Table VIII. The values of x_m and w obtained in this experiment are listed in columns 4 and 5 of Table VIII.

In general, the distribution has a negative region at small depths (see Figs. 2–6). This is caused by excess of secondary emission over deposition of the incident electrons. The main feature of the

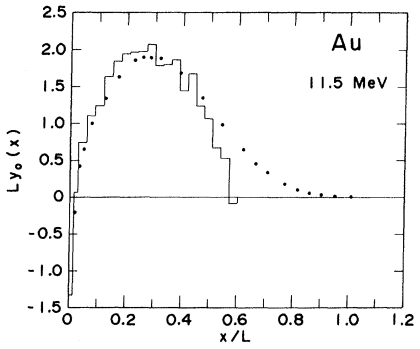

FIG. 6. Measured charge distribution of 11.5-MeV electrons in Au is shown by solid circles. Histogram represents the Monte Carlo result of Berger and Seltzer for 10 MeV and the Pb slab of thickness 0.6L.

TABLE III. Charge distribution $y(x)$ produced by 4.09-MeV electrons in the absorbers of Be, Al, Cu, Ag, and Au. The absorber thickness x is expressed in units of g/cm^2, and $y(x)$ is in 10^{-1} cm^2/g absorbed electron.

Be($Z=4$)		Al($Z=13$)		Cu($Z=29$)		Ag($Z=47$)		Au($Z=79$)	
x	$y(x)$	x	$y(x)$	x	$y(x)$	x	$y(x)$	x	$y(x)$
0.071	−1.6	0.072	−0.73	0.065	−0.72	0.071	0.24	0.073	0.48
0.173	−0.603	0.124	0.183	0.083	0.475	0.093	1.67	0.167	5.06
0.265	−0.288	0.207	0.794	0.156	2.06	0.179	3.83	0.272	7.53
0.448	0.046	0.344	1.58	0.335	3.89	0.276	5.19	0.366	8.87
0.642	0.524	0.479	2.37	0.511	5.34	0.384	6.43	0.449	9.72
0.825	0.943	0.614	3.04	0.621	6.16	0.481	7.36	0.543	10.07
0.971	1.45	0.749	4.21	0.781	7.14	0.614	7.99	0.648	10.08
1.17	2.52	0.886	5.10	0.949	7.60	0.722	8.36	0.742	9.34
1.35	3.70	1.02	6.08	1.13	7.47	0.819	8.43	0.825	8.58
1.54	5.45	1.16	6.79	1.40	6.06	0.927	8.01	1.05	6.33
1.72	7.33	1.29	7.42	1.57	4.79	1.02	7.57	1.25	4.14
1.82	8.21	1.45	7.72	1.84	2.57	1.25	5.72	1.42	2.39
1.94	9.30	1.59	7.55	2.01	1.21	1.45	3.81	1.62	1.23
2.04	9.53	1.72	6.86	2.11	0.769	1.68	2.08	1.80	0.520
2.14	9.32	1.86	5.49	2.28	0.258	1.89	0.958	2.01	0.205
2.24	8.72	1.99	4.13	2.37	0.124	2.09	0.329	2.21	0.052
2.32	7.92	2.05	3.33	2.46	0.070	2.31	0.091	2.39	0.033
2.42	5.94	2.13	2.37	2.55	0.032	2.51	0.027	2.59	0.026
2.45	5.19	2.18	1.88	2.72	0.022	2.74	0.015	2.77	0.015
2.51	3.93	2.27	1.12						
2.55	3.13	2.32	0.789						
2.61	1.97	2.40	0.383						
2.65	1.34	2.45	0.229						
2.69	1.14	2.54	0.027						
2.73	0.906								
2.79	0.282								
2.83	0.165								
2.84	0.128								
2.87	0.062								

distribution is a rather broad peak centered at about 20–90% of L. Behavior of the peak as the incident-electron energy E_0 or the atomic number Z of the absorber is varied can be discussed conveniently by using the parameters x_m and w.

Figure 7 is a plot of the ratio x_m/L vs E_0. The results obtained for Al by Gross and Wright[13] and

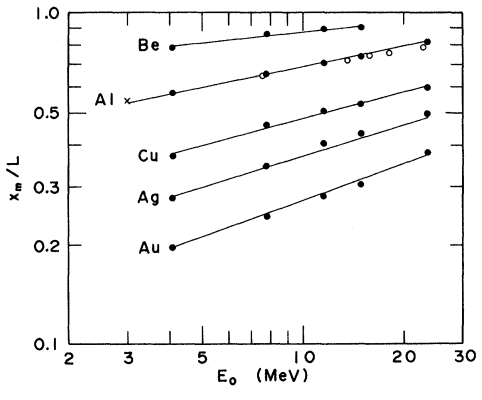

FIG. 7. Ratio of the most probable charge-deposition depth x_m to the mean range L of the incident electrons plotted as a function of incident energy E_0. Dark circles represent present data; a cross represents data of Gross and Wright, Ref. 13; open circles represent data of Alexander *et al.*, Ref. 14. Solid lines represent results of least-squares fit to the present data with Eq. (6).

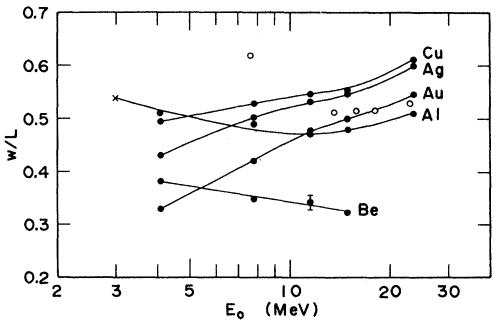

FIG. 8. Ratio of the charge-deposition straggling w to the mean range L of the incident electrons plotted as a function of incident energy E_0. Dark circles represent present data; a cross represents data of Gross and Wright, Ref. 13; open circles represent data of Alexander *et al.* (Al), Ref. 14. Smooth curves connect experimental values.

TABLE IV. Charge distribution $y(x)$ produced by 7.79-MeV electrons in the absorbers of Be, Al, Cu, Ag, and Au. The absorber thickness x is expressed in units of g/cm^2, and $y(x)$ is in 10^{-1} cm^2/g absorbed electron.

Be ($Z=4$)		Al ($Z=13$)		Cu ($Z=29$)		Ag ($Z=47$)		Au ($Z=79$)	
x	$y(x)$	x	$y(x)$	x	$y(x)$	x	$y(x)$	x	$y(x)$
0.091	−1.5	0.100	−1.1	0.102	−0.91	0.114	−0.31	0.104	−0.24
0.193	−0.738	0.231	−0.305	0.138	−0.187	0.222	0.731	0.143	0.889
0.468	−0.336	0.372	−0.032	0.281	0.563	0.319	1.40	0.198	1.57
1.19	0.069	0.642	0.333	0.548	1.33	0.524	2.11	0.303	2.36
1.96	0.584	0.914	0.694	0.986	2.26	0.765	2.78	0.480	3.32
2.70	1.57	1.18	1.06	1.43	3.20	0.970	3.34	0.679	4.08
3.22	2.96	1.48	1.63	1.87	3.85	1.18	3.72	0.856	4.56
3.60	4.18	1.75	2.21	2.05	3.94	1.39	3.98	1.08	4.86
3.82	4.87	2.02	2.81	2.23	3.90	1.59	4.19	1.28	4.89
4.02	5.40	2.29	3.43	2.50	3.87	1.84	4.11	1.45	4.73
4.20	5.59	2.56	3.94	2.94	3.25	2.04	3.93	1.65	4.34
4.39	5.49	2.80	4.28	3.11	2.79	2.24	3.67	2.04	3.42
4.57	4.85	3.07	4.39	3.38	2.09	2.56	3.02	2.34	2.62
4.72	3.96	3.34	4.21	3.82	1.06	2.90	2.32	2.62	1.84
4.92	2.64	3.61	3.63	4.09	0.546	3.31	1.36	2.89	1.22
5.10	1.41	3.88	2.71	4.27	0.344	3.72	0.626	3.22	0.670
5.29	0.541	4.18	1.59	4.50	0.141	4.17	0.183	3.77	0.169
5.39	0.235	4.31	1.15	4.68	0.066	4.37	0.091	3.98	0.095
5.47	0.151	4.45	0.680	4.86	0.025	4.58	0.041	4.18	0.053
5.57	0.051	4.58	0.416	5.13	0.006	4.78	0.014	4.36	0.027
5.67	0.018	4.72	0.221					4.56	0.019
		4.85	0.094					4.74	0.006
		4.99	0.034						
		5.13	0.009						

by Alexander *et al.*[14] are also shown in this figure, and are in good agreement with the present results. As can be seen from Fig. 7, x_m/L decreases with decreasing E_0 and with increasing Z, and can be expressed by a power function of E_0 in the energy region of the present experiment:

$$x_m/L = AE_0^B , \tag{6a}$$

where A and B are constants for each absorber. An analysis shows that these may be given by

$$A = a_1/(Z + a_2) , \tag{6b}$$

$$B = a_3(Z - a_4)^{a_5} , \tag{6c}$$

where the a_i's ($i = 1, 2, 3, \ldots, 5$) are constants. Values of these constants determined from least-squares fit to the present data are listed in Table IX.

The ratio w/L is plotted as a function of E_0 in Fig. 8. It increases with increasing E_0 in the region of $E_0 \gtrsim 11$ MeV for Al and in the entire energy region of the present experiment for Cu, Ag, and Au. Values of w/L measured by the previous authors for Al are again shown for comparison. While the results of Gross and Wright are quite consistent with the present data, those of Alexander *et al.* are considerably larger. The latter authors have not given any discussion of the instrumental width in their measurements. The effect of this width can probably account for the discrepancy.

The charge distributions at large depths are expected to reflect the following contributing phenomena: (i) multiple scattering detours of the primary electrons; (ii) energy-loss straggling of the primary electrons; (iii) deposition of electrons mediated by bremsstrahlung. The mean-squares deflection of electrons due to multiple scattering increases with decreasing E_0 and increasing Z. This increase in deflection will cause shortening of the penetration depth, and accordingly will cause a shift of x_m/L toward smaller values. Such an effect of the first phenomenon is clearly reflected in the trend of x_m/L described above.

The second phenomenon affects the charge-deposition straggling w. The aforementioned increase of w/L with increasing E_0 is considered to reflect mainly the increasing effect of bremsstrahlung energy-loss straggling. Similar increase of width can be seen in the path-length distributions calculated by Blunck[23] for electrons of energies higher than 1 MeV passing through the Pb absorber.

Another effect caused by the second phenomenon is the appearance of a sort of Gaussian terminal trend. When the energy-loss straggling is small, the path-length distribution of electrons is nearly a Gaussian curve centered at the length of L.[23] Therefore, "remains" of this distribution are expected to be seen for the cases in which the effect

TABLE V. Charge distribution $y(x)$ produced by 11.5-MeV electrons in the absorbers of Be, Al, Cu, Ag, and Au. The absorber thickness x is expressed in units of g/cm^2, and $y(x)$ is in 10^{-1} cm^2/g absorbed electron.

Be($Z=4$)		Al($Z=13$)		Cu($Z=29$)		Ag($Z=47$)		Au($Z=79$)	
x	$y(x)$	x	$y(x)$	x	$y(x)$	x	$y(x)$	x	$y(x)$
0.14	−1.3	0.13	−1.0	0.12	−0.84	0.14	−0.48	0.13	−0.35
0.33	−0.536	0.18	−0.645	0.57	0.378	0.19	0.060	0.22	0.731
1.04	−0.107	0.32	−0.354	1.00	0.866	0.34	0.536	0.32	1.13
2.01	0.076	0.54	−0.146	1.46	1.27	0.68	1.13	0.50	1.74
2.57	0.247	0.94	0.089	1.89	1.77	1.21	1.84	0.80	2.33
2.95	0.371	1.35	0.306	2.34	2.20	1.75	2.48	1.10	2.83
3.51	0.636	1.78	0.607	2.77	2.53	2.27	2.78	1.47	3.22
3.85	0.879	2.19	0.927	2.95	2.66	2.52	2.90	1.67	3.28
4.44	1.45	2.59	1.33	3.23	2.74	2.81	2.81	1.85	3.27
4.97	2.15	2.96	1.72	3.40	2.77	3.34	2.64	2.07	3.26
5.38	2.81	3.37	2.25	3.66	2.68	3.88	2.10	2.54	2.93
5.72	3.31	3.78	2.64	4.11	2.50	4.40	1.49	3.04	2.34
5.90	3.53	4.21	3.05	4.33	2.31	4.94	0.857	3.51	1.72
6.10	3.83	4.62	3.17	4.78	1.91	5.36	0.484	4.01	1.13
6.28	3.95	5.02	3.08	5.39	1.19	5.90	0.190	4.30	0.795
6.47	3.93	5.43	2.61	5.67	0.861	6.43	0.060	4.58	0.576
6.61	3.77	5.76	1.99	5.84	0.666	6.68	0.031	4.98	0.312
6.79	3.39	6.17	1.24	6.10	0.434	6.97	0.015	5.27	0.176
6.94	3.11	6.36	0.882	6.28	0.312	7.23	0.007	5.55	0.108
7.13	2.54	6.57	0.552	6.55	0.147			5.83	0.051
7.36	1.91	6.76	0.318	6.73	0.101			6.14	0.025
7.41	1.56	7.00	0.137	6.98	0.045			6.52	0.010
7.51	1.28	7.19	0.059	7.16	0.023				
7.61	0.915	7.41	0.019						
7.68	0.765	7.68	0.003						
7.79	0.497								
7.91	0.323								
8.01	0.182								
8.08	0.119								
8.18	0.064								
8.28	0.030								
8.38	0.019								

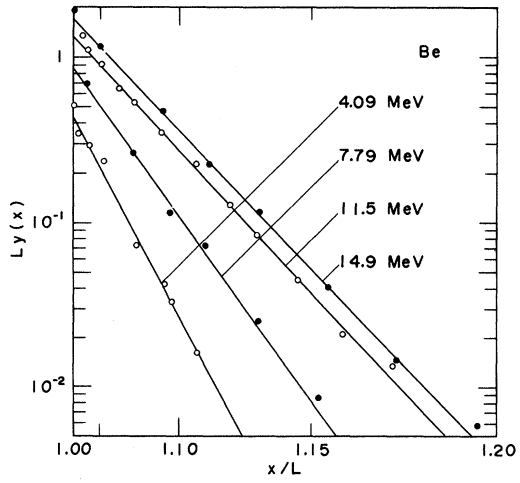

FIG. 9. Charge distributions of electrons at the depths $x>L$ are plotted in quadratic and logarithmic scales, showing a Gaussian terminal trend. Straight lines represent results of least-squares fit to the data with Eq. (7). The absorber is Be, and the incident energies are 4.09, 7.79, 11.5, and 14.9 MeV.

of the first phenomenon is also not so strong as to distort the path-length distribution to a high degree. Analysis of the present data shows that in the cases of Be and Al absorbers (except the case of 4.09-MeV electrons in Al for which only a single data point was observed for $x>L$) the tail of the charge distribution for $x>L$ is, to a good approximation, expressed by right-side half of a Gaussian curve beginning from $x=L$. This is illustrated for Be in Fig. 9. The straight lines in this figure represent least-squares fit to the data with

$$y(x)=b_1 e^{-(x-L)^2/2b_2^2}, \tag{7}$$

where b_1 and b_2 are constants for each curve. In fitting this equation, the single point nearest to $x=L$ in each of the distributions for 4.09, 11.5, and 14.9 MeV has been excluded, because deviation from the Gaussian trend apparently occurs in the proximity of L. It is to be noted that the main distribution, as distinct from the tail, is not Gaussian.

The third phenomenon will give an exponential tail of the distribution dominated by the absorption

TABLE VI. Charge distribution $y(x)$ produced by 14.9-MeV electrons in the absorbers of Be, Al, Cu, Ag, and Au. The absorber thickness x is expressed in units of g/cm^2, and $y(x)$ is in 10^{-1} cm^2/g absorbed electron.

Be($Z=4$)		Al($Z=13$)		Cu($Z=29$)		Ag($Z=47$)		Au($Z=79$)	
x	$y(x)$	x	$y(x)$	x	$y(x)$	x	$y(x)$	x	$y(x)$
0.17	−1.1	0.17	−0.92	0.17	−0.87	0.19	−0.51	0.18	−0.35
0.37	−0.541	0.30	−0.462	0.62	0.129	0.40	0.238	0.39	0.665
0.74	−0.293	0.43	−0.307	1.05	0.424	0.73	0.636	0.56	1.03
1.11	−0.187	0.71	−0.153	1.50	0.723	1.26	1.10	0.76	1.31
2.06	−0.035	1.25	0.031	1.94	1.01	1.80	1.58	1.16	1.81
2.98	0.091	1.81	0.218	2.39	1.31	2.32	1.95	1.53	2.21
3.90	0.247	2.36	0.423	2.82	1.66	2.86	2.23	1.73	2.41
4.80	0.520	2.87	0.687	3.27	1.91	3.39	2.32	2.12	2.62
5.73	0.976	3.41	0.987	3.71	2.15	3.93	2.25	2.33	2.62
6.44	1.59	3.95	1.36	4.16	2.25	4.45	2.05	2.50	2.62
6.96	2.15	4.51	1.77	4.38	2.25	4.99	1.69	2.70	2.58
7.34	2.55	5.06	2.14	4.83	2.22	5.41	1.36	2.88	2.54
7.77	3.07	5.53	2.40	5.26	2.09	5.95	0.956	3.10	2.46
8.12	3.23	6.07	2.54	5.71	1.82	6.48	0.617	3.30	2.35
8.31	3.21	6.61	2.43	6.15	1.54	7.02	0.343	3.47	2.25
8.49	3.20	7.17	2.00	6.60	1.17	7.54	0.171	3.67	2.10
8.74	2.92	7.45	1.70	7.03	0.858	8.08	0.071	4.06	1.76
9.02	2.53	7.72	1.37	7.48	0.523	8.61	0.026	4.44	1.43
9.21	2.10	7.99	1.05	7.92	0.306	9.15	0.009	5.04	0.972
9.57	1.26	8.23	0.757	8.37	0.145			5.41	0.686
9.95	0.513	8.49	0.466	8.80	0.061			6.00	0.377
10.14	0.245	8.77	0.257	9.21	0.023			6.38	0.246
10.32	0.127	9.04	0.122	9.64	0.013			6.98	0.111
10.52	0.044	9.31	0.048					7.35	0.052
10.70	0.016	9.58	0.014					7.94	0.023
10.89	0.006	9.87	0.006					8.32	0.012
								8.92	0.005

coefficient of the x rays with the highest significant energy in the bremsstrahlung spectrum. This exponential tail is expected to be seen in a semilogarithmic plot as a straight line attained after gradual decrease of the gradient. In the actual distributions, however, the gradient of the decaying slope does not clearly show such decrease up to the deepest points observed. While in most cases of

TABLE VII. Charge distribution $y(x)$ produced by 23.5-MeV electrons in the absorbers of Al, Cu, Ag, and Au. The absorber thickness x is expressed in units of g/cm^2, and $y(x)$ is in 10^{-1} cm^2/g absorbed electron.

Al($Z=13$)		Cu($Z=29$)		Ag($Z=47$)		Au($Z=79$)	
x	$y(x)$	x	$y(x)$	x	$y(x)$	x	$y(x)$
0.29	−0.78	0.29	−0.59	0.33	−0.34	0.32	−0.21
0.83	−0.128	1.17	0.109	0.87	0.271	0.69	0.518
2.17	0.113	2.94	0.630	1.40	0.494	1.29	0.928
3.55	0.312	4.50	1.09	2.46	0.908	1.76	1.21
5.58	0.722	5.38	1.29	3.53	1.30	2.26	1.45
7.19	1.16	6.27	1.45	4.59	1.53	2.73	1.67
8.30	1.41	7.15	1.44	5.13	1.57	3.23	1.80
9.37	1.61	8.04	1.35	5.55	1.58	3.70	1.84
10.87	1.38	8.88	1.19	6.62	1.41	4.20	1.82
11.41	1.17	9.76	0.914	7.68	1.09	5.17	1.60
12.48	0.657	10.65	0.616	8.75	0.736	6.14	1.20
13.02	0.432	11.53	0.373	9.81	0.417	7.11	0.775
13.59	0.185	12.42	0.153	10.83	0.178	8.08	0.453
14.13	0.091	13.09	0.067	11.90	0.060	9.05	0.217
		13.97	0.014	12.96	0.015	10.02	0.091
						10.99	0.028

TABLE VIII. Values of the mean range L of the incident electrons, the most probable charge-deposition depth x_m, and the charge-deposition straggling w.

Absorber	E_0 (MeV)	L[a] (g/cm^2)	x_m (g/cm^2)	w (g/cm^2)
Be	4.09	2.59	2.04 ± 0.02	0.99 ± 0.03
(Z = 4)	7.79	4.92	4.23 ± 0.03	1.71 ± 0.09
	11.5	7.14	6.36 ± 0.04	2.44 ± 0.10
	14.9	9.11	8.20 ± 0.05	2.94 ± 0.11
Al	4.09	2.53	1.45 ± 0.02	1.29 ± 0.02
(Z = 13)	7.79	4.66	3.04 ± 0.04	2.28 ± 0.07
	11.5	6.62	4.65 ± 0.06	3.12 ± 0.10
	14.9	8.27	6.10 ± 0.07	3.96 ± 0.10
	23.5	11.98	9.80 ± 0.17	6.11 ± 0.34
Cu	4.09	2.73	1.01 ± 0.03	1.35 ± 0.06
(Z = 29)	7.79	4.87	2.23 ± 0.04	2.57 ± 0.11
	11.5	6.73	3.40 ± 0.03	3.68 ± 0.13
	14.9	8.22	4.36 ± 0.05	4.55 ± 0.11
	23.5	11.42	6.80 ± 0.12	6.98 ± 0.31
Ag	4.09	2.83	0.785 ± 0.017	1.22 ± 0.04
(Z = 47)	7.79	4.88	1.69 ± 0.03	2.45 ± 0.08
	11.5	6.58	2.66 ± 0.04	3.50 ± 0.14
	14.9	7.91	3.42 ± 0.07	4.32 ± 0.14
	23.5	10.67	5.32 ± 0.07	6.40 ± 0.27
Au	4.09	2.97	0.585 ± 0.016	0.98 ± 0.04
(Z = 79)	7.79	4.93	1.20 ± 0.03	2.07 ± 0.06
	11.5	6.47	1.81 ± 0.03	3.09 ± 0.06
	14.9	7.64	2.33 ± 0.03	3.82 ± 0.13
	23.5	9.99	3.80 ± 0.07	5.45 ± 0.20

[a]Reference 22.

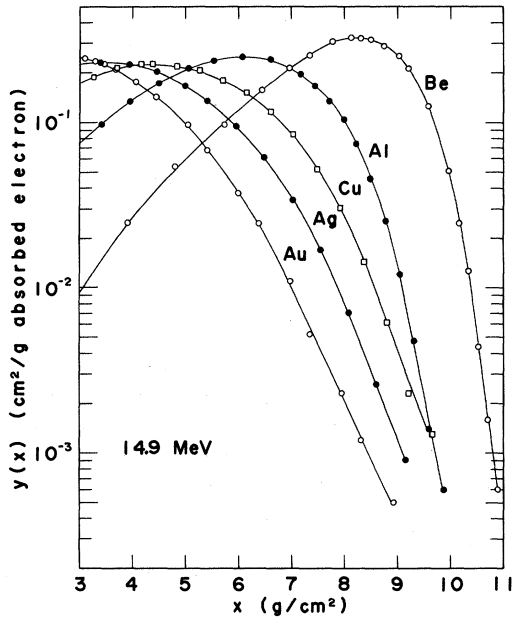

FIG. 10. Charge distributions of electrons at deep penetration are shown in semilogarithmic plot. The incident energy is 14.9 MeV, and the absorbers are Be, Al, Cu, Ag, and Au. Smooth curves connect experimental values.

$E_0 \leq 14.9$ MeV the slope becomes essentially a straight line after gradual *increase* of the gradient (see Fig. 10), it corresponds to an absorption coefficient larger than 1 cm^2/g, which is much larger than the absorption coefficient of the x rays in the MeV region. It can be concluded from these facts that the distributions at the largest depths of the present experiment are not yet dominated by the electrons mediated by bremsstrahlung. The contribution of these electrons to the distributions observed is, therefore, less than about 1×10^{-3} cm^2/g absorbed electron.

The Monte Carlo results of Berger and Seltzer[18] are compared with the present experiment in Figs. 2–6. Although the incident energy of 10 MeV assumed for the calculation is different from the experimental energy of 11.5 MeV, this difference is unimportant because of the rather slow change with energy of the distribution expressed in parameters of x/L and $Ly_0(x)$ (see Figs. 3, 7, and 8). Similarly, the difference between Au and Pb absorbers in Fig. 6 is not so important. It is also to be noted that the calculations for 10-MeV electrons in Al, Cu, Ag, and Pb assumed slab absorbers with thicknesses given in the captions of Figs. 3–6, respectively, whereas the experimental data are in all cases for semi-infinite media. The effect of this geometrical difference appears only near the transmission surface, where the Monte Carlo values are lower than the experimental results, as expected; the higher values in the semi-infinite configuration are due to backscattering of electrons from deeper layers.

In Fig. 2, results of two Monte Carlo programs are shown; in the one, the energy loss of electrons was treated in the continuous slowing-down approximation (the dashed histogram), and in the other, energy-loss straggling was taken into account (the solid histogram). It can be seen that agreement with experiment is much improved by including energy-loss straggling. All the Monte Carlo results in Figs. 3–6 were generated by the latter program. Histories of secondary knock-on electrons are followed by the programs used, so that the negative

TABLE IX. Values of constants in the empirical equation for x_m/L. Errors attached are those of least-squares fit.

Constant	Value
a_1	8.14 ± 0.39
a_2	8.86 ± 0.84
a_3	0.110 ± 0.007
a_4	3.10 ± 0.28
a_5	0.275 ± 0.015

TABLE X. Comparison of the experimental and calculated values of the fraction $F(x; Z, E_0)$ of the charge deposited at the depths larger than x.

Z	E_0 (MeV)	x	$F(x; Z, E_0)$ Experimental	Calculated[a]
4	10	$0.9L$	0.316 ± 0.012	0.41
13	4	$0.5L$	0.552 ± 0.021	0.54

[a] Reference 18.

values of the distribution at small depths are well reproduced in the calculated results. On the whole, the calculated distributions are rather in good agreement with the experimental results except for the geometrical effect aforementioned and a discrepancy remaining for Be. This discrepancy will be examined below.

Recently Lonergan *et al.*[24] have measured energy spectra of electrons transmitted through targets of Be, Al, and Au for incident energies of 4.0 and 8.0 MeV, and have compared the results with calculations generated by the same computer program of Berger and Seltzer as that used in obtaining the results quoted in the present paper. In this comparison, two discrepancies have been found: (i) Calculated spectrum of 8.0-MeV electrons after passing through a Be target of $0.5L$ thickness was shifted approximately 250 keV above the measured spectrum. (ii) The number of 4.0-MeV electrons transmitted through an Al slab of $0.5L$ thickness was 25% higher in the calculation. Thus, Lonergan *et al.* concluded that the Monte Carlo calculation might have a tendency to generate deeper penetration for low Z absorbers. This conclusion suggests that the calculated charge distributions of electrons in Be and Al may be shifted toward larger depths compared with experiment. For Be, the following discrepancy can be inspected from Fig. 2: The calculated distribution shows lower values than the measured distribution at the depths of $0.4-0.7L$, and attains considerably higher values around the peak, causing deeper average penetration. On the other hand, no appreciable difference can be seen from Fig. 3 in the case of 4-MeV electrons in Al. In order to confirm these inspections, it will be helpful to evaluate the fraction $F(x; Z, E_0)$ of the charge deposited at the depths larger than x:

$$F(x; Z, E_0) = \int_x^\infty y_0(x')\, dx'. \tag{8}$$

Values of $F(0.9L; 4, 10 \text{ MeV})$ and $F(0.5L; 13, 4 \text{ MeV})$ for the experimental and calculated distributions are shown in Table X. The experimental value for 10-MeV electrons in Be has been determined through interpolation from values for the experimental energies. In the case of Be, the Monte Carlo value is larger than the experimental value by about 30%, clearly indicating the higher penetrability in the calculation. This is consistent with the conclusion of Lonergan *et al.* However, the peaks of the experimental and calculated charge distributions occur at about the same values of x/L, and it is not obvious whether this discrepancy in F has a close connection with the spectral shift. For 4-MeV electrons in Al, the two values of F agree within the experimental error, and this is contradictory to the second discrepancy found by Lonergan *et al.* Therefore, the presence, suggested by them, of the tendency of the calculation resulting in higher penetrability is not supported by the present data in the case of Al.

ACKNOWLEDGMENTS

The authors would like to express their appreciation to Dr. K. Kimura, the president of RCO, and Dr. T. Azuma for their encouragement throughout the course of this work. They would also like to thank Dr. M. Y. Nakai who kindly arranged the loan of Be absorbers from Osaka Laboratory, Japan Atomic Energy Research Institute. Thanks are due to the members of the linear accelerator groups of RCO and KURRI for their kind cooperation. Finally the authors wish to thank M. Hayashi for his valuable aid in carrying out the computor calculations of least-squares fit.

[1] R. D. Birkhoff, in *Handbuch der Physik*, edited by S. Flügge (Springer, Berlin, 1958), Vol. 34, p. 53.

[2] J. E. Leiss, S. Penner, and C. S. Robinson, Phys. Rev. 107, 1544 (1957).

[3] T. Sidei, T. Higasimura, and K. Kinosita, Mem. Fac. Eng., Kyoto Univ. 19, 220 (1957).

[4] J. F. Perkins, Phys. Rev. 126, 1781 (1962).

[5] M. J. Berger, in *Methods in Computational Physics*, edited by B. Adler, S. Fernbach, and M. Rotenbert (Academic, New York, 1963), Vol. 1, p. 135.

[6] M. J. Berger and S. M. Seltzer, National Aeronautics and Space Administration Report No. NASA SP-71, 1965 (unpublished), p. 437.

[7] B. W. Mar, Nuclear Sci. Eng. 24, 193 (1966).

[8] M. J. Berger and S. M. Seltzer, National Aeronautics and Space Administration Report No. NASA SP-169, 1968 (unpublished), p. 285.

[9] S. Wittig, Johann-Wolfgang-Goethe University Institute for Nuclear Physics Report No. IKF-20, 1968 (unpublished).

[10] M. J. Berger and S. M. Seltzer, Ann. Acad. Sci. (N. Y.) 161, 8 (1969).

[11] N. D. Kessaris, Phys. Rev. 145, 164 (1966).

[12] L. V. Spencer, Phys. Rev. 98, 1597 (1955).

[13] B. Gross and K. A. Wright, Phys. Rev. 114, 725 (1959).

[14] W. Alexander, A. Brynjolfsson, and R. D. Cooper, U. S. Army Natic Laboratories Technical Report No. FD-2 1964 (unpublished).

[15] J. S. Laughlin, in *Symposium on High-Energy Electrons*, edited by A. Zuppinger and G. Poretti (Springer, Berlin, 1965), p. 11.

[16]T. Tabata, R. Ito, and S. Gkabe, Ann. Rep. Rad. Center Osaka Prefect. 9, 34 (1968).
[17]T. Tabata, R. Ito, S. Okabe, and Y. Fujita, Ann. Rep. Rad. Center Osaka Prefect. 10, 34 (1969).
[18]M. J. Berger and S. M. Seltzer (private communication); calculation carried out with program ETRAN developed at the National Bureau of Standards. The basic features of this program are described in Refs. 5, 8, and 10.
[19]T. Tabata, Phys. Rev. 162, 336 (1967).
[20]D. Harder and H. Metzger, Z. Naturforsch. 23a, 1675 (1968).
[21]P. J. Ebert, A. F. Lauzon, and E. M. Lent, Phys. Rev. 183, 422 (1969).
[22]M. J. Berger and S. M. Seltzer, National Aeronautics and Space Administration Report No. NASA SP-3012, 1964 (unpublished).
[23]O. Blunck, Z. Physik 131, 354 (1952).
[24]J. A. Lonergan, C. P. Jupiter, and G. Merkel, J. Appl. Phys. 41, 678 (1970).

PHYSICAL REVIEW B VOLUME 3, NUMBER 3 1 FEBRUARY 1971

Stochastic Theory of Line Shape: Off-Diagonal Effects in Fine and Hyperfine Structure*

M. J. Clauser
Sandia Laboratories, Albuquerque, New Mexico 87115
and
M. Blume
Physics Department, Brookhaven National Laboratory, Upton, New York 11973
(Received 14 September 1970)

An extension of the stochastic model of relaxation effects is used to derive a theory of the line shape of fine and hyperfine structure. The theory is developed for Mössbauer spectra, but can be readily applied in related fields such as perturbed angular correlations, electron and nuclear spin resonance, and optical spectroscopy. Previous stochastic-model theories of hyperfine spectra have used a semiclassical fluctuating-field approach which inherently restricts the hyperfine Hamiltonian to matrix elements which are diagonal with respect to the electronic states. In the present theory, these restrictions are removed by using a quantum-mechanical treatment of the combined electronic-nuclear system, wherein the relaxation enters as random instantaneous transitions between electronic states. This allows inclusion of the effects of off-diagonal electronic hyperfine matrix elements (e.g., the pseudoquadrupole interaction). A model for the relaxation is presented which allows all the transition rates to be specified independently, as is necessary to treat finite temperatures. Two examples are used to illustrate the the theory and to compare it with other theories.

I. INTRODUCTION

Numerous stochastic[1–5] and *ab initio*[6–10] treatments of the effects of time-dependent perturbations on Mössbauer line shapes have appeared in recent years. Many of these theories are derived from similar developments in magnetic resonance[11–13] or perturbed angular correlations,[14–16] and they are applicable in many other line-shape problems as well. In this paper, we present a generalization of the stochastic theories to cover a class of situations not previously discussed.[17]

A simple illustration shows the type of extension made. In stochastic treatments of Mössbauer line shape, the hyperfine interaction between the nuclear spin and the electronic spin is replaced by an interaction between the nuclear spin and randomly varying external magnetic and electric fields.[18] The randomly varying fields represent the effect of a relaxing electronic spin on the nucleus. This type of treatment is only valid, however, if the electronic part of the hyperfine interaction has no off-diagonal matrix elements, since an external magnetic field has no such elements. Thus, such a treatment is reasonable for a hyperfine interaction of the form aI_zS_z, since the electronic relaxation causes a time dependence to be induced in S_z, which is a diagonal operator. If the interaction is of the form $a\vec{I}\cdot\vec{S}$, however, we may not replace $\vec{S}$ by a varying external field. The appropriate time-varying field would be of the form $\vec{h}(t)=a\langle\psi(t)|\vec{S}|\psi(t)\rangle$. Since, in the stochastic model, $\psi(t)$ jumps instantaneously from one electronic state to another, $\vec{h}(t)$ only takes on the values $a\langle i|\vec{S}|i\rangle$, and the off-diagonal matrix elements $\langle i|\vec{S}|j\rangle$ would be ignored. These matrix elements are important when the splitting of the electronic levels is not large compared with the hyperfine splitting. Our approach here is to treat the entire nucleus-electron system quantum mechanically. The effects of electronic relaxation are then introduced by additional terms in the Hamiltonian which have random properties and which are capable of inducing transitions between the different electronic levels. Previous